Received: 2 May 2016 | Revised: 5 July 2016 | Accepted: 27 July 2016

DOI 10.1002/qua.25225

FULL PAPER

WILEY International Journal of QUANTUM CHEMISTRY

The electron delocalization range in stretched bonds

Arshad Mehmood | Benjamin G. Janesko

Department of Chemistry and Biochemistry, Texas Christian University, 2800 S. University Dr, Fort Worth, Texas 76129

Correspondence
Arshad Mehmood, Department of Chemistry and Biochemistry, Texas Christian University, 2800 S. University Dr, Fort Worth, Texas 76129.
Email: arshad.mehmood@tcu.edu

Abstract

The electron delocalization range function EDR($\vec{r}, d$) (Janesko et al., *J. Chem. Phys.* 2014, 141, 144104) quantifies the width of the one-particle density matrix about point $\vec{r}$, measuring aspects of delocalization. Here, we explore the EDR in stretched and compressed chemical bonds. The EDR illustrates how compressing chemical bonds localizes the one-particle density matrix about the reference point, and captures aspects of fractional occupancy, and left-right correlation in stretched covalent bonds.

KEYWORDS

bond dissociation, correlation, delocalization

1 | INTRODUCTION

Electron delocalization is fundamental to our understanding of chemical bonding. Chemistry students are taught how valence electrons delocalize across covalent bonds, and how bond breaking returns electrons to atoms. Visualizing, quantifying, and interpreting aspects of bonding remains a topic of active study. Novel bonding motifs, from sigma aromaticity[1] to sigma-hole[2] and charge-shift[3] bonding, are regularly proposed in the literature. New electronic structure approximations attack classic problems, including nondynamical correlation[4–6] and dissociation of odd-electron[4,7,8] and multiple bonds.[9,10]

Many theorists have built computational tools to help understand bonding based on electronic structure calculations. Some tools are computed directly from calculated *N*-electron wavefunctions. Examples include weights of resonance structures,[11] valence bond theory,[12] block-localized wavefunctions,[13] natural bond orbitals,[14] sharing indices,[15] and adaptive natural density partitioning.[16] Other tools are calculated from the electron density, including the quantum theory of atoms in molecules,[17,18] inhomogeneity,[19] bond ellipticity,[20] and the single exponential decay detector.[21]

We focus on tools built from the nonlocal one-particle density matrix (1-RDM) $\gamma(\vec{r},\vec{r}')$, obtained from *N*-electron wavefunction $\Psi(\vec{r}_1,\vec{r}_2\ldots\vec{r}_n)$ as

$$\begin{aligned}\gamma(\vec{r},\vec{r}') &= N\int d^3\vec{r}_2\ldots d^3\vec{r}_N\Psi(\vec{r},\vec{r}_2\ldots\vec{r}_n)\Psi^*(\vec{r}',\vec{r}_2\ldots\vec{r}_n)\\ &= \sum_i n_i\varphi_i(\vec{r})\varphi_i^*(\vec{r}')\end{aligned} \quad (1)$$

(Spin dependence is suppressed for conciseness) Diagonal 1-RDM elements $\rho(r) = \lim_{\vec{r}'\to\vec{r}}\gamma(\vec{r},\vec{r}')$ give the probability density for finding an electron at point *r*. Like molecular orbitals $\varphi_i(\vec{r})$ themselves, off-diagonal 1-RDM elements $\vec{r}\neq\vec{r}'$ are not quantum-mechanical observables. However, many previous authors have shown how these nonobservable quantities can provide insight into chemical bonding.[22,23] The interference effects of atomic orbitals may be more apparent in the off-diagonal part of 1-RDM than in the diagonal charge density.[22,24] The electronic kinetic energy expectation value is an explicit function of the 1-RDM but not of the electron density.[25,26] The 1-RDM contributes to the electron pair density through the Fermi hole ($\propto|\gamma(\vec{r},\vec{r}')|^2$).[27,28] The off-diagonal parts of the 1-RDM show positive and negative peaks and saddle points which arise from chemical bonds and do not occur in promolecular 1-RDM.[22,29] The off-diagonal elements of the 1-RDM in Hilbert space yields various definitions of covalent bond order.[30–32] The off-diagonal elements are indirectly linked to momentum-space description of chemical system and provide information about the velocity and "range" of electrons.[22]

The electron delocalization range function is designed to address an inherent problem of analyzing the 1-RDM: namely, that this function of six variables cannot be visualized all at once. The EDR is designed to extract information about bonding out of the full 1-RDM. To motivate our analysis, therefore, we provide a brief overview of some other methods to extract information about bonding out of the full 1-RDM. Two-dimensional plots of the 1-RDM along symmetry axes has been achieved to characterize and classify the various off-diagonal regions.[22,23] Such analyses are particularly useful for transition density matrices.[33–35] Orbital and basis-set independent bond orders[27,28,36–40] have been obtained by the integration of the 1-RDM, its square root, or the Fermi hole over atomic domains.[18] The domain-averaged Fermi holes, which provides the quantitative assessment of

electron delocalization, location and degree of electrons pairing, energy ordering of resonance structures and finer details of electron–electron interactions are obtained by partial integration over atomic domains.[27,41,42] Direct partitioning of the 1-RDM into *pairs* of atomic domains provides useful information about covalent bond orders, bond polarization, transferability, bonding multiplicity, and contribution of individual atoms to covalent bonds which in turn quantify the dative nature of bonds.[43–45] The kinetic energy density[27] in positive definite form, which is (as stated above) an explicit function of the 1-RDM but not of the electron density, provides the electron localization function (ELF),[46–49] the localization and delocalization indices count the number of electrons shared between atoms,[50] the noncovalent interaction index,[51] the source function,[52] electron population analysis-based electron delocalization index[53] and electron localizability indicator.[54] Electron sharing indices from different partition schemes based on density matrices have highlighted the effect of correlation in polar, nonpolar and aromatic systems.[55] The localized orbital locator, reciprocal form factor and parity function obtained by projecting the off-diagonal 1-RDM onto the subspaces of internal or external coordinates, provide complementary analysis of molecular electronic structure.[56–58] Perhaps most pertinent to the present work, analyses of the projected Fermi hole provide insight into the interplay of exchange hole delocalization and strong correlation in dissociating bonds.[59–62]

The electron delocalization range function EDR$(\vec{r};d)$ complements these tools by focusing on the *distance* between points *r* and *r*′ in $\gamma(\vec{r},\vec{r}')$. The EDR quantifies the extent to which the 1-RDM about point *r* decays over *r*-*r*′ with distance *d*. It does so by projecting $\gamma(\vec{r},\vec{r}')$ onto a *model* 1-RDM that is centered at point *r*, and decays over *r*-*r*′ with distance *d*, *by construction*:

$$\mathrm{EDR}(\vec{r};d) = \int d^3\vec{r}'\, g_d(\vec{r},\vec{r}')\gamma(\vec{r},\vec{r}') \tag{2}$$

$$g_d(\vec{r},\vec{r}') = \rho^{-\frac{1}{2}}(\vec{r})\left(\frac{2}{\pi d^2}\right)^{3/4}\exp\left(-\frac{|\vec{r}-\vec{r}'|^2}{d^2}\right) \tag{3}$$

Equation 3 is the 1-RDM of a well-defined reference system, a uniform electron gas (UEG) with density $\rho \sim d^{-3}$.[63] (More precisely, *Equation* 3 is a Gaussian fit to the exact Kohn–Sham density matrix of the UEG, constructed to remove Friedel oscillations.) This ensures $|EDR(\vec{r};d)| \leq 1$. The projection is conceptually related to the spatial distribution of odd electrons obtained from the exchange hole normalization,[61,62] as well as to recent extensions incorporating projection onto a localized model exchange hole.[60,61]

Figure 1 of reference 64 shows how the EDR quantifies the off-diagonal width of the 1-RDM about reference point *r*. Reference 63 presents the equations necessary to evaluate *Equation* 2. We have used the EDR to quantify the delocalization of atoms and molecules,[63] solvated electrons,[64] and electrides.[65] The atomic averages of the EDR and plots of EDR on molecular surfaces provide a chemically intuitive picture of the sizes of occupied orbital lobes in different regions of molecule.[66] The topological analysis of EDR provides useful information about chemistry of molecules, solids, and surfaces.[67] Preliminary investigations of H_2 dissociation illustrated how the EDR can quantify the interplay of delocalization and nondynamical correlation, the fractional

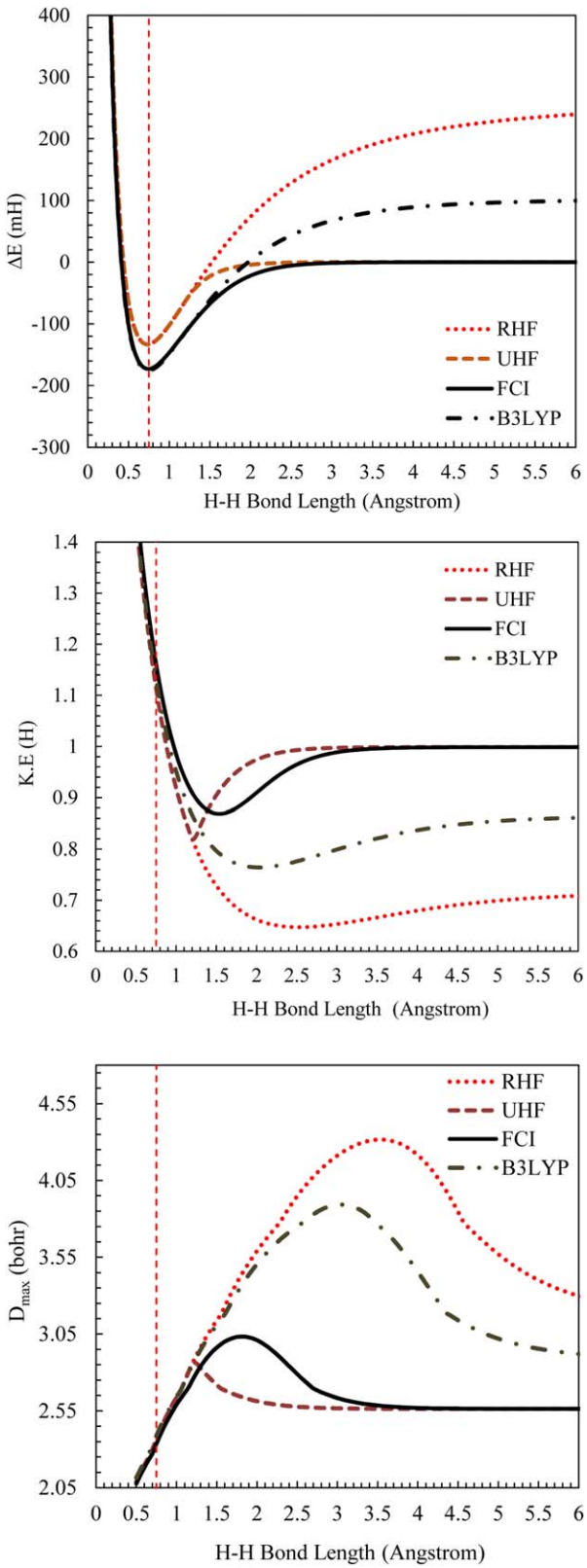

FIGURE 1 Bond dissociation energy ΔE_{bond}, (top), electronic kinetic energy expectation value KE, (middle), and system-averaged delocalization length D_{max} (bottom) of ground-state singlet H_2, plotted versus H—H bond length

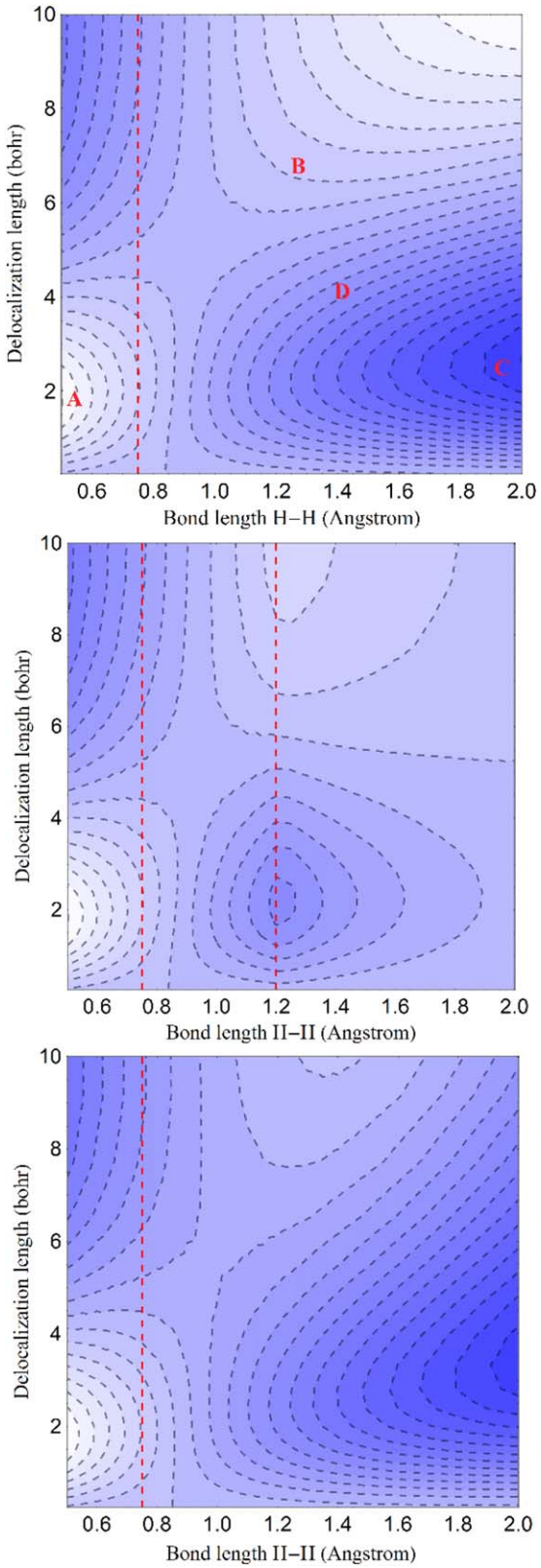

FIGURE 2 Bond delocalization shift $\Delta\overline{\mathrm{EDR}}(H_2;d)$ of ground-state singlet H_2, plotted versus delocalization distance d and H—H bond length. RHF (top), UHF (middle), FCI (bottom). Horizontal lines denote the equilibrium bond length and Coulson–Fischer point

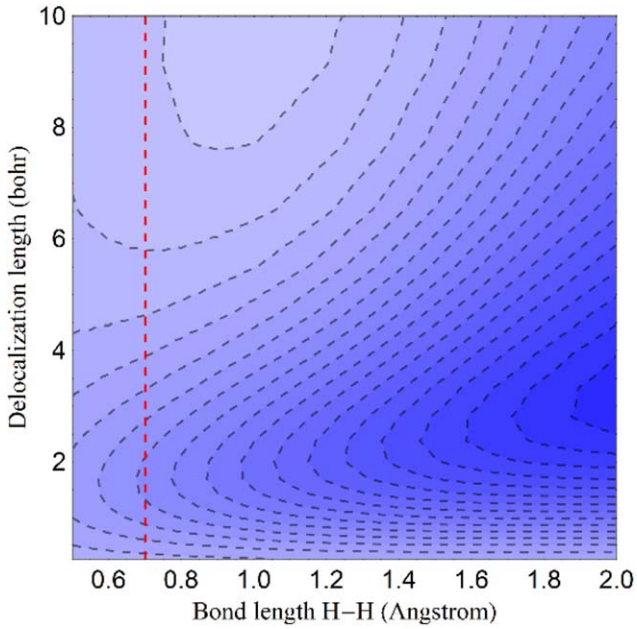

FIGURE 3 FCI bond delocalization shift $\Delta\overline{\mathrm{EDR}}(H_2;d)$ of ground-state singlet H_2, evaluated in a minimal basis set

occupations ("fractional spin")[68,69] at dissociation, and the errors made by restricted and unrestricted Hartree–Fock (UHF) theory. This work extends those studies by treating other bonding situations including closed-shell interactions, polar covalent, charge-shift, and ionic bonds.

As a function of four variables, the EDR cannot be visualized in its entirety. We instead use three different "descriptors" extracted from the EDR. *Descriptor 1* is the "system-averaged delocalization length"

$$D_{\max} = \mathrm{argmax}(d)\ \overline{\mathrm{EDR}}(d) \tag{4}$$

built from the system-averaged

$$\overline{\mathrm{EDR}}(d) = \int d^3\vec{r}\,\rho(\vec{r})\mathrm{EDR}(\vec{r};d). \tag{5}$$

In general, as a system's electrons become more diffuse and weakly bound, their average kinetic energy decreases and $D_{\max}$ increases. We plot system's total kinetic energy and $D_{\max}$ versus bond length for a global picture of how bond stretching delocalizes electrons.

Descriptor 2 is the "bond delocalization shift," defined as how a molecule's $\overline{EDR}(d)$ differs from its separate atoms. Diatomic A-B has:

$$\Delta\overline{\mathrm{EDR}}(AB;d) = \overline{\mathrm{EDR}}(d)AB - \overline{\mathrm{EDR}}(d)A\ -\overline{\mathrm{EDR}}(d)B \tag{6}$$

Two-dimensional plots of bond delocalization shift as a function of delocalization length d (bohr) and bond length R (Å) illustrate how bonding localizes the 1-RDM. Compressing bonds tends to localize electrons, giving a positive bond delocalization shift at small distances d, and a negative bond delocalization shift at large d.

Descriptor 3 is real-space plots of isosurfaces EDR(r;d_{special}) evaluated at "special" length scales d_{special}. This shows the locations in real space where electrons tend to be localized to distance d_{special}. For example, our study of electrons solvated in water clusters[64] chose d_{special} to maximize $\Delta\overline{\mathrm{EDR}}(AB;d)$ of the cluster with versus without a solvated electron. The resulting EDR(r;d_{special}) highlighted precisely the

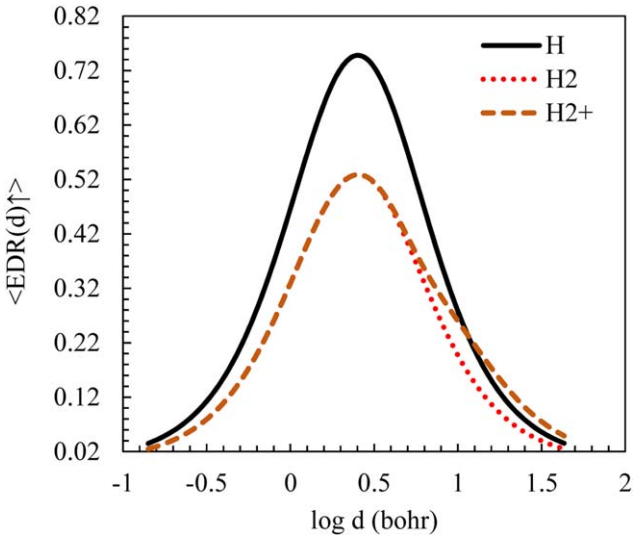

FIGURE 4 System averaged $\overline{\mathrm{EDR}}(d)$ of H atom, stretched FCI H_2, and stretched H_2^+

same region of space as the major lobe of the orbital containing the solvated electron. This choice of "special" length scale itself had a one-to-one correlation with the solvated electron's HOMO radius of gryration, demonstrating how Descriptor 3 extracts chemically relevant information about 1-RDM localization. We also include contour plots of EDR(*x*,*d*) for points x along a bond axis, a convention introduced in reference 63.

2 | COMPUTATIONAL DETAILS

Calculations use restricted Hartree–Fock (RHF) theory, unrestricted Hartree-Fock (UHF), coupled cluster theory (CCSD), Kohn–Sham density functional theory (DFT) with the B3LYP exchange-correlation functional,[70–75] or full configuration interaction (FCI) providing the exact ground state in a given basis set. Unrestricted calculations use stability analysis to locate stable wavefunctions.[76] CCSD density matrices are evaluated using the Z-vector approach.[77,78] Molecular orbitals are expanded in the aug-*cc*-pVTZ[79,80] basis set unless noted otherwise. No corrections are made for basis set superposition error. All calculations use the development version of the Gaussian suite of programs.[81] The EDR is evaluated as described previously.[63–65] $D_{\max}$ is evaluated by numerical maximization of $\overline{\mathrm{EDR}}(d_i)$ evaluated on an even-tempered set of 10–60 distances d_i. Calculations were performed using quadratically convergent SCF procedures.[82] ΔEDR plots along with other useful information are provided in Supporting Information. ΔE_{bond} and KE denote the bond dissociation energy and the electronic kinetic energy expectation value.

3 | RESULTS AND DISCUSSION

3.1 | Ground-state singlet H_2

The H_2 molecule's singlet ground state is the textbook illustration of left-right electron correlation.[83] Stretching the bond beyond the

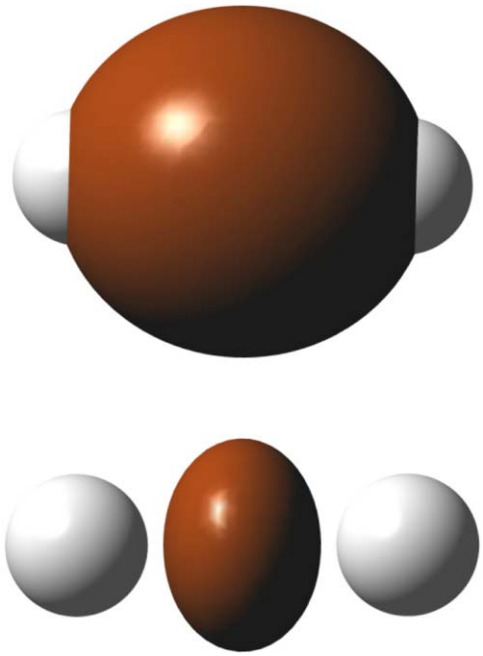

FIGURE 5 EDR $(\vec{r}, d = 4.0\ \text{bohr}) = 0.75$ for H_2 stretched to bond length 1.4Å. (top) RHF, (bottom) FCI

Coulson–Fischer bond length makes the RHF wavefunction unstable, leading to a symmetry breaking that localizes spin-up and spin-down electrons to different atoms. Further stretching makes the RHF singlet and UHF triplet energy curves cross. Accurate treatments of the stretched bond require multireference calculations, which may be thought of as incorporating the two Lewis structures $H^{\uparrow}H^{\downarrow}$ and $H^{\downarrow}H^{\uparrow}$.[4] Previous studies have shown that ELF could not effectively visualize these effects, as the ELF from single-determinant calculations on H_2 is identically 1 at all points in space and at all bond lengths.[67,84] Basin-point sharing indices and the shared-electron distribution index clearly highlight the interplay of delocalization and correlation in this system.[38,41] Critical points in the off-diagonal 1-RDM are associated with the covalent bond.[23]

We begin by extending our previous study[63] of H_2. Figure 1 shows a global picture of H_2 dissociation, plotting the bond energy ΔE_{bond}, total electronic kinetic energy KE, and system-averaged delocalization length $D_{\max}$ as functions of bond length. ΔE_{bond} and KE match previous work.[85–91] Trends in $D_{\max}$ mirror trends in KE: where the KE is large, $D_{\max}$ is small, and vice versa. At the equilibrium bond length, the exact (FCI) KE is larger than that of two H atoms consistent with the virial theorem.[92–94]

Stretching the bond gives a KE minimum at modest bond lengths,[95] and convergence to the isolated atom limit. RHF calculations predict an excessively large $D_{\max}$ and excessively low KE at dissociation. This is a well-known consequence of RHF theory's nonzero probability for finding both electrons on the same atom at dissociation, a spurious Coulomb repulsion that produces a spuriously over-delocalized density matrix and a spurious low KE. Symmetry-restricted RB3LYP DFT calculations partly correct for this over-delocalization. UHF calculations show a derivative discontinuity in KE and $D_{\max}$ at the Coulson–Fischer point, and "over-localization" with too small $D_{\max}$ and

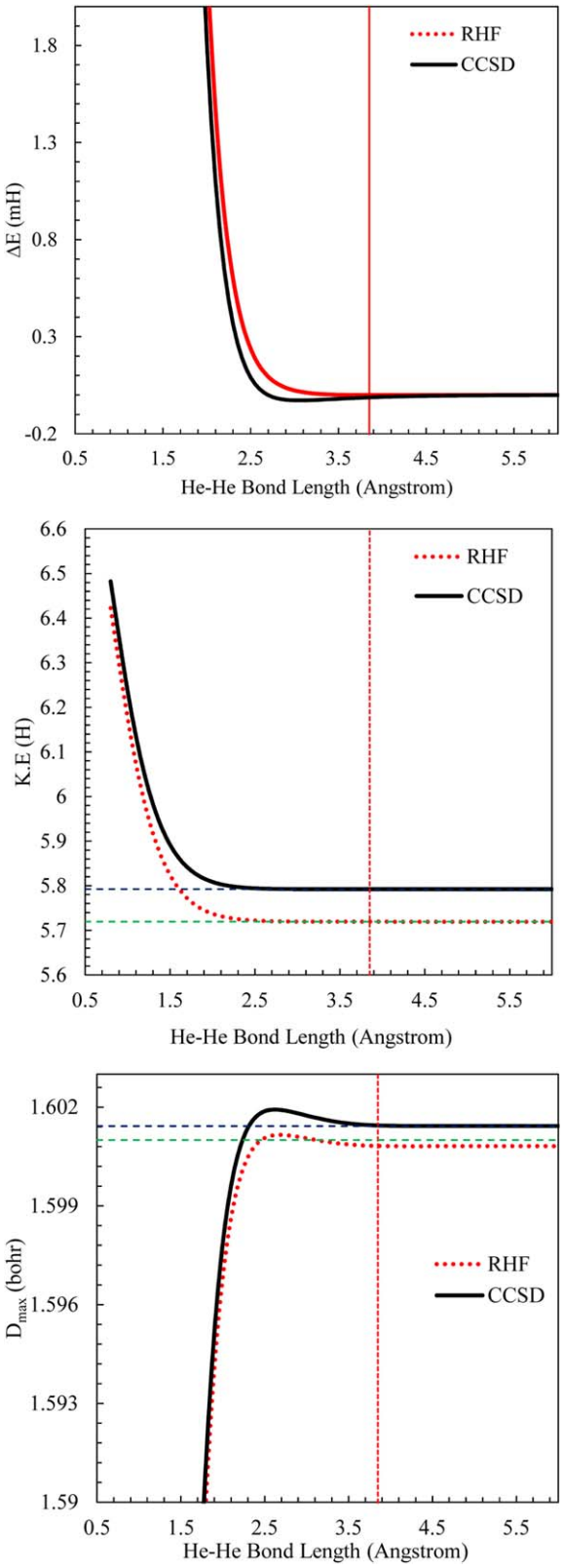

FIGURE 6 ΔE_{bond}, KE, and D_{max} of ground-state singlet He_2, plotted versus He—He bond length. Vertical dotted line denotes the equilibrium bond length. Horizontal dotted line denotes the value for two isolated He atoms

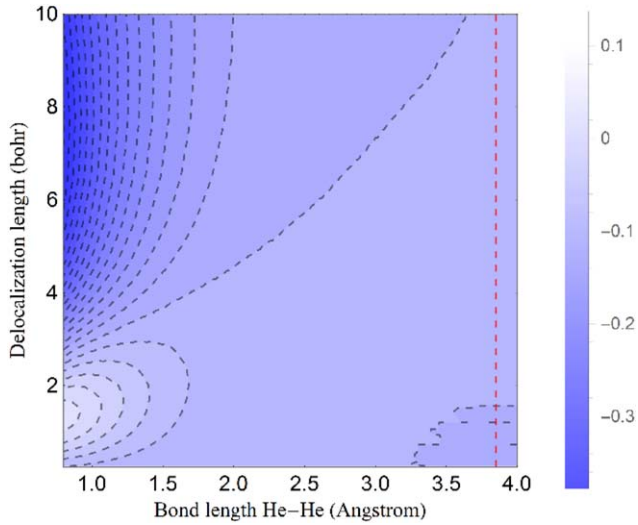

FIGURE 7 CCSD bond delocalization shift $\Delta\overline{\mathrm{EDR}}(He_2; d)$ for He_2, plotted as a function of delocalization distance d and He—He bond length. Small numerical artifacts at small d and large bond length arise from our choice of contours

too large KE at bond lengths around 2 Angstrom. This reproduces the recent study by Hollett and coworkers, who found that the UHF kinetic energy of correlation is negative in this region.[5]

Figure 2 shows how the ↑-spin electron's bond delocalization shift $\Delta\overline{\mathrm{EDR}}(H_2; d)$ gives more insight into dissociation. Test calculations on H_2^+ give a bond delocalization shift qualitatively similar to H_2 (not shown). At equilibrium, the electrons are more localized[95] and more tightly bound than in the isolated atoms, giving a positive peak at small delocalization distance d (Figure 2a region A) and a negative peak at large d. Compressing the bond further localizes the electrons and intensifies these peaks.

Before continuing, we highlight an example of how the bond delocalization shift can visualize a classic concept in chemical bonding. Figure 3 shows how the bond delocalization shift highlights the well-known contraction of the electron density towards the nuclei in covalent bonds.[92–94] Minimal-basis calculations that prevent density contraction yield an overall delocalization of the electrons at equilibrium: unlike the large-basis calculations in Figure 2a, the electrons are more delocalized than in the isolated atoms, giving a negative peak at small d and a positive peak at large d. This analysis isolates the critical role of delocalization in covalent bonding.

Returning to Figure 2, we see that the bond delocalization shift can also help visualize the "fractional spin" critical to nondynamical correlation in chemical bonds.[96] This highlights the EDR's connections to recent studies of effectively unpaired electrons based on projected exchange holes.[59–62] At stretched bond lengths, both RHF and FCI calculations give that the ↑-spin electron has an equal probability of being found on either the left or right atom. Projecting this *delocalized* electron's 1-RDM onto the *localized* 1-RDM of *Equation* 2 gives a value much less than 1, *regardless* of distance d. This shows up as a dark (negative) region growing in at large bond lengths (Figure 2a point C). This region of the bond delocalization shift thus precisely identifies the fractional occupancy of atoms in a dissociated covalent bond. Figure 4

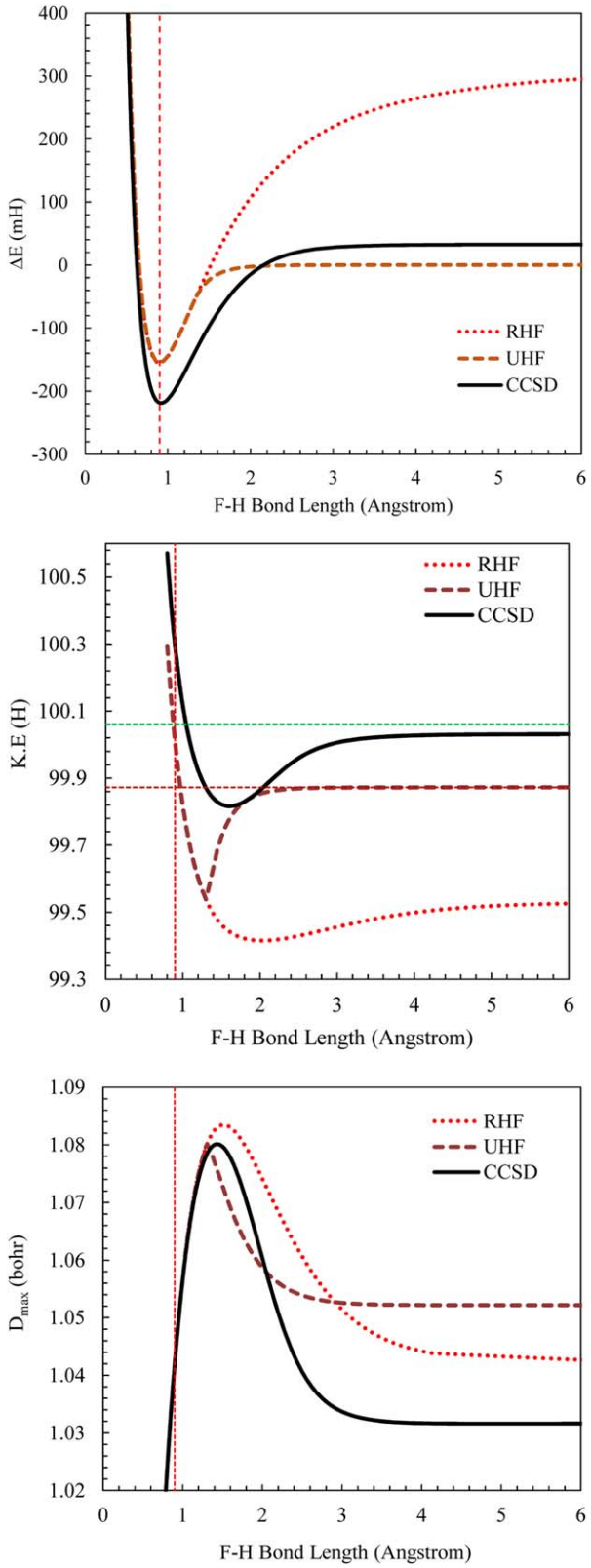

FIGURE 8 ΔE_{bond}, KE, and D_{max} of ground-state singlet FH molecule, plotted versus F—H bond length. Vertical line denotes equilibrium bond length. Horizontal lines denote the sum of isolated H and F atoms for CCSD and UHF

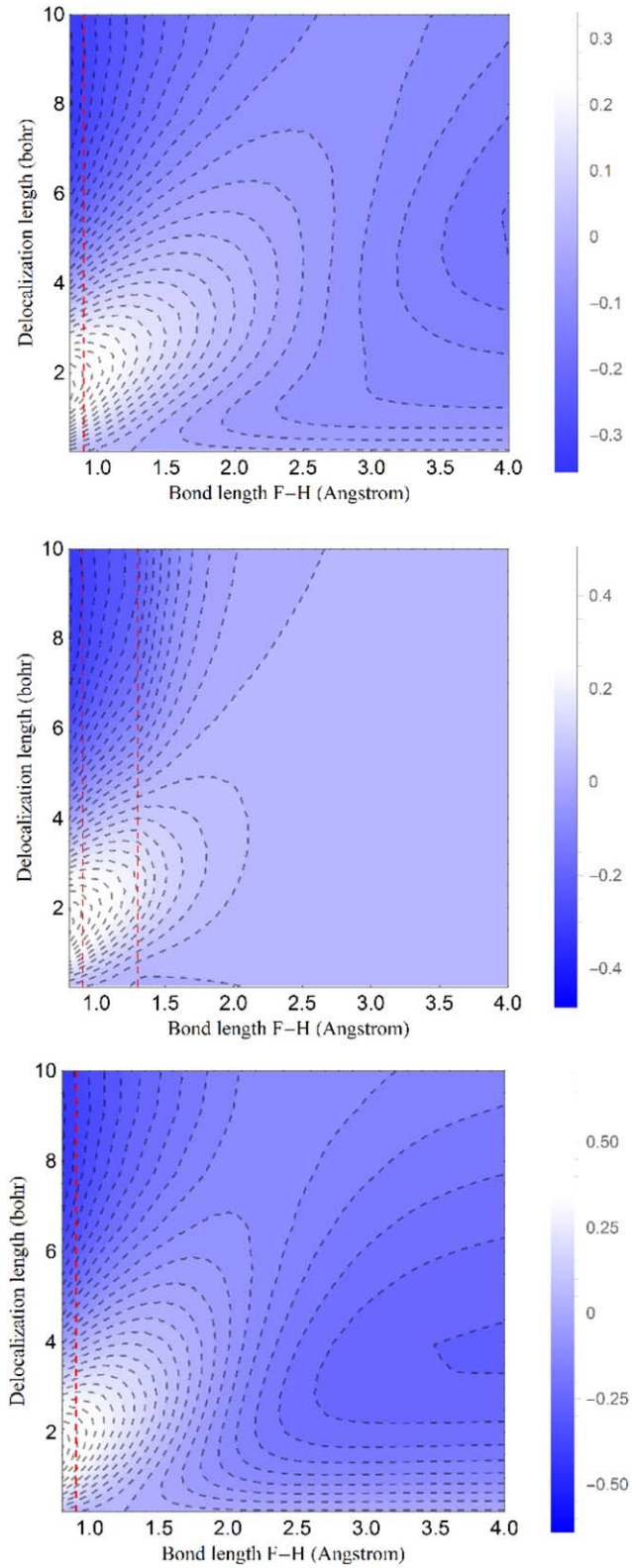

FIGURE 9 Bond delocalization shift $\Delta\overline{EDR}(FH;d)$ of FH plotted as a function of delocalization distance d and F—H bond length. RHF (top), UHF (middle), CCSD (bottom). Dotted line denotes the equilibrium bond length and Coulson–Fischer point

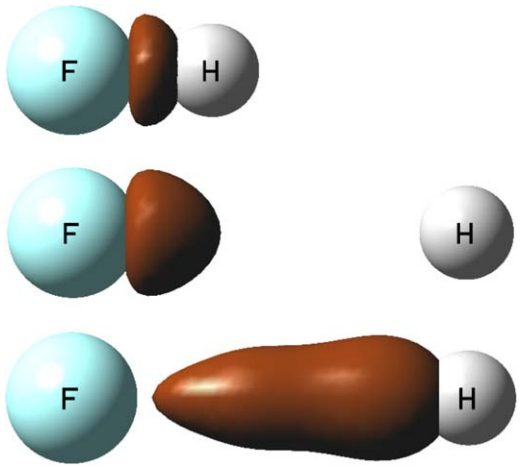

FIGURE 10 Isosurfaces of the RHF EDR in F—H molecule. (Top) EDR$(\vec{r}, d = 2$ bohr$) = 0.7$ at equilibrium bond length. (Middle) EDR $(\vec{r}, d = 2$ bohr$) = 0.7$ at bond length 2.5 Å. (Bottom) EDR $(\vec{r}, d = 4$ bohr$) = 0.5$ at bond length 2.5Å

provides an additional proof of this effect, showing the system-averaged EDR itself for H atom and dissociated H_2 and H_2^+. The two dissociated bonds have half spin-up electron on each atom, which rescales the entire system-averaged $\overline{\mathrm{EDR}}(d)$ by a factor of $1/\sqrt{2}$. (A small "bump" at very large d arises from the finite bond lengths used here.) This result clearly illustrates how the positive and negative regions of the bond delocalization shift highlight the interplay of bond stretching and fractional occupancy in dissociating bonds. Moreover, the UHF bond delocalization shift in Figure 2 smoothly converges to zero past the Coulson–Fischer point, highlighting the *absence* of fractional occupancy effects in the symmetry-broken calculation.

The RHF and FCI bond delocalization shifts in Figure 2 have a small positive peak at all plotted bond lengths. The distance d of this peak increases with bond length (Figure 2 region B). This peak arises from overlap between the density matrix on the atoms and the EDR test function at the bond midpoint.

While system-averaged values like those plotted in Figures 2–4 suffice for insight into simple diatomics, analyses of bonding in more complicated molecules will require a real-space picture of the effects of stretching individual bonds. We thus conclude our discussion of H_2 by showing how our third descriptor can provide such a real-space picture. Figure 5 shows the real-space EDR from point "D" in Figure 2a: relatively large distance $d = 4$ Bohr, bond length R stretched to 1.4 Angstrom. The RHF isosurface shows that these relatively delocalized electrons reside near the middle of the bond, as expected from conventional pictures of chemical bonding. Plots of the EDR at $d = 1$ Bohr and the equilibrium bond length are qualitatively similar (Supporting Information). The FCI isosurface also sits near the bond midpoint, but occupies a smaller volume, consistent with RHF over-delocalization.

3.2 | van der Waals interaction: He_2

Helium dimer has a weak van der Waals interaction.[97] van der Waals interactions arise from electron pair fluctuations, and will not show up in the 1-RDM. Topological analysis identifies a weakly antibonding

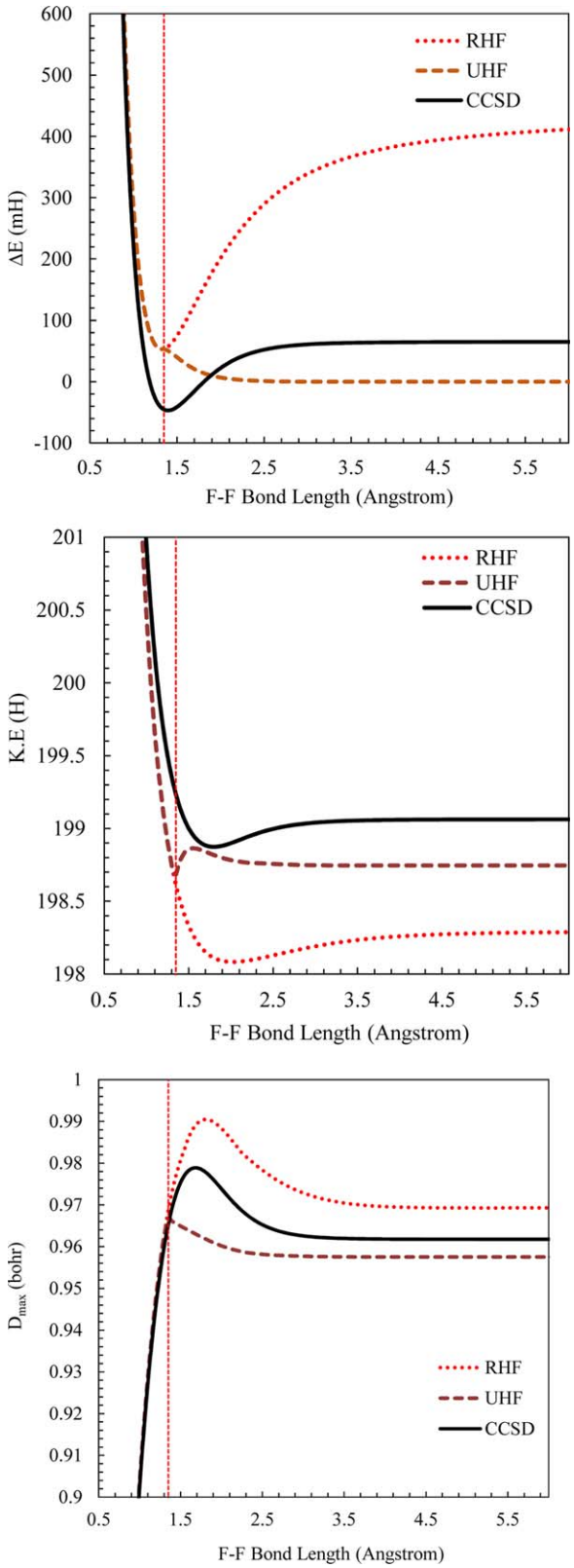

FIGURE 11 ΔE_{bond}, KE, and D_{max} of ground-state singlet F_2, plotted versus F—F bond length

interaction in the He_2 1-RDM, as distinct from the coupled fluctuations of electron pair probability giving rise to the van der Waals interaction.[23] The electron sharing index decays exponentially with distance,

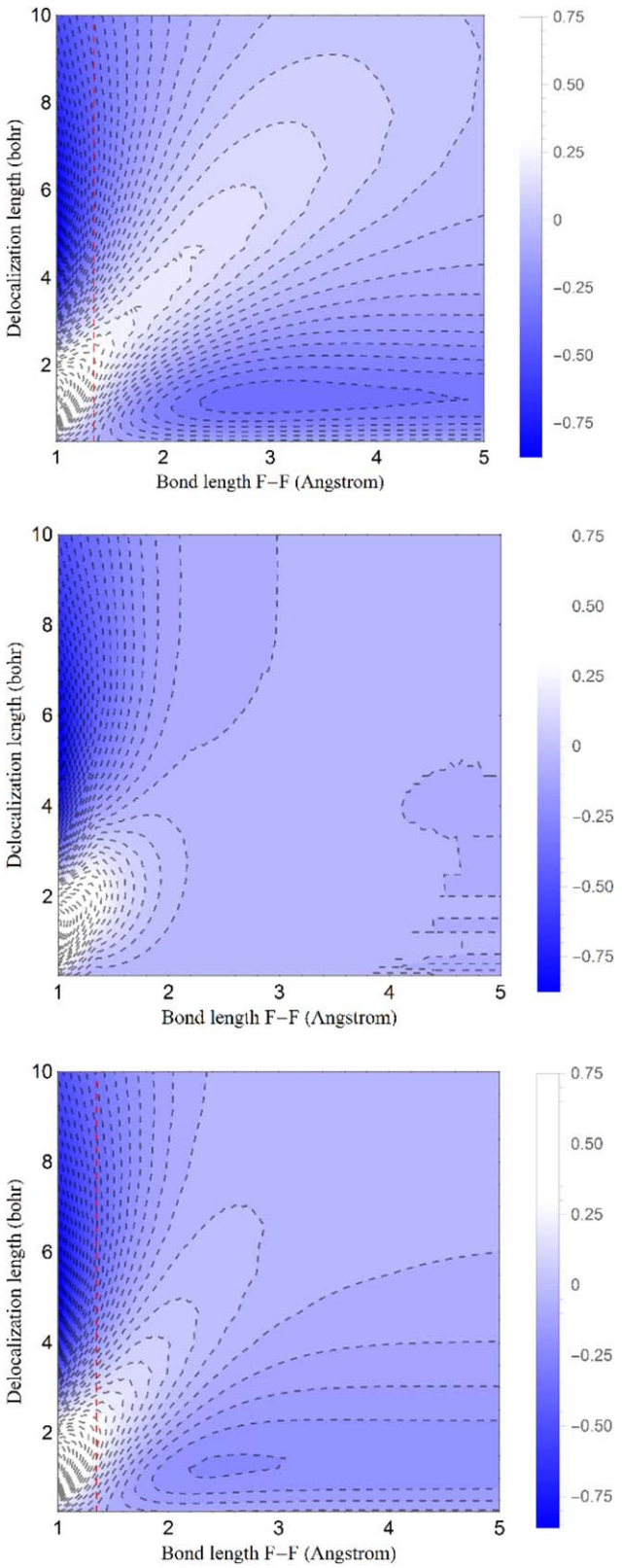

FIGURE 12 Bond delocalization shift $\Delta\overline{\mathrm{EDR}}(F_2;d)$ of F_2 plotted as a function of delocalization distance d and F—F bond length. RHF (top), UHF (middle), CCSD (bottom). Dotted line denotes RHF local minimum bond length

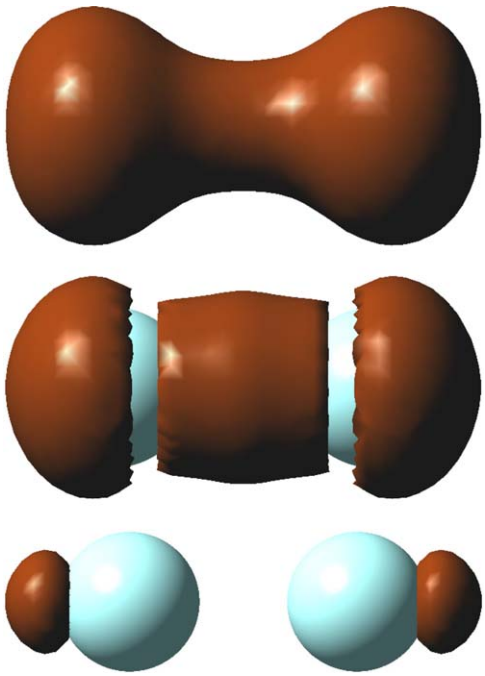

FIGURE 13 Isosurfaces of the CCSD EDR in F_2, at the RHF local minimum bond length 1.30 Å. (Top) EDR $(\vec{r}, d = 1.00\ \text{bohr}) = 0.8$. Middle EDR $(\vec{r}, d = 1.50\ \text{bohr}) = 0.75$ (Bottom) EDR $(\vec{r}, d = 3.00\ \text{bohr}) = 0.45$

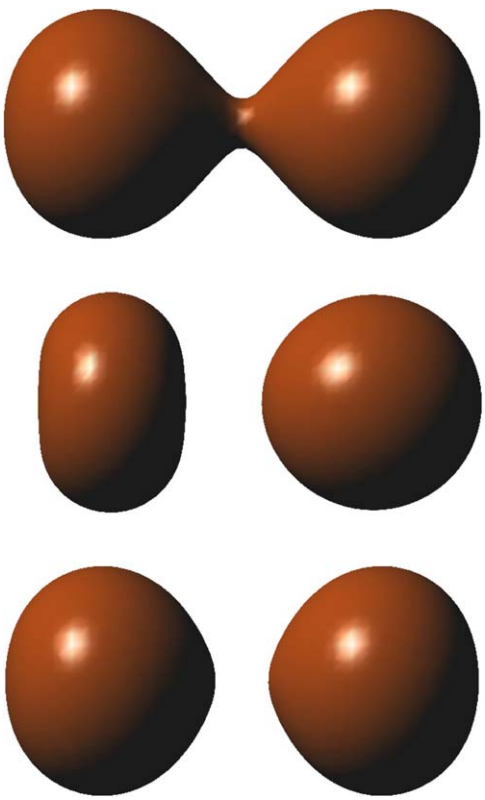

FIGURE 14 Isosurfaces EDR$(\vec{r}, d = 1.00\ \text{bohr}) = 0.6$ in F_2 stretched to bond length 2.00Å. (Top) RHF, (middle) UHF, (bottom) CCSD

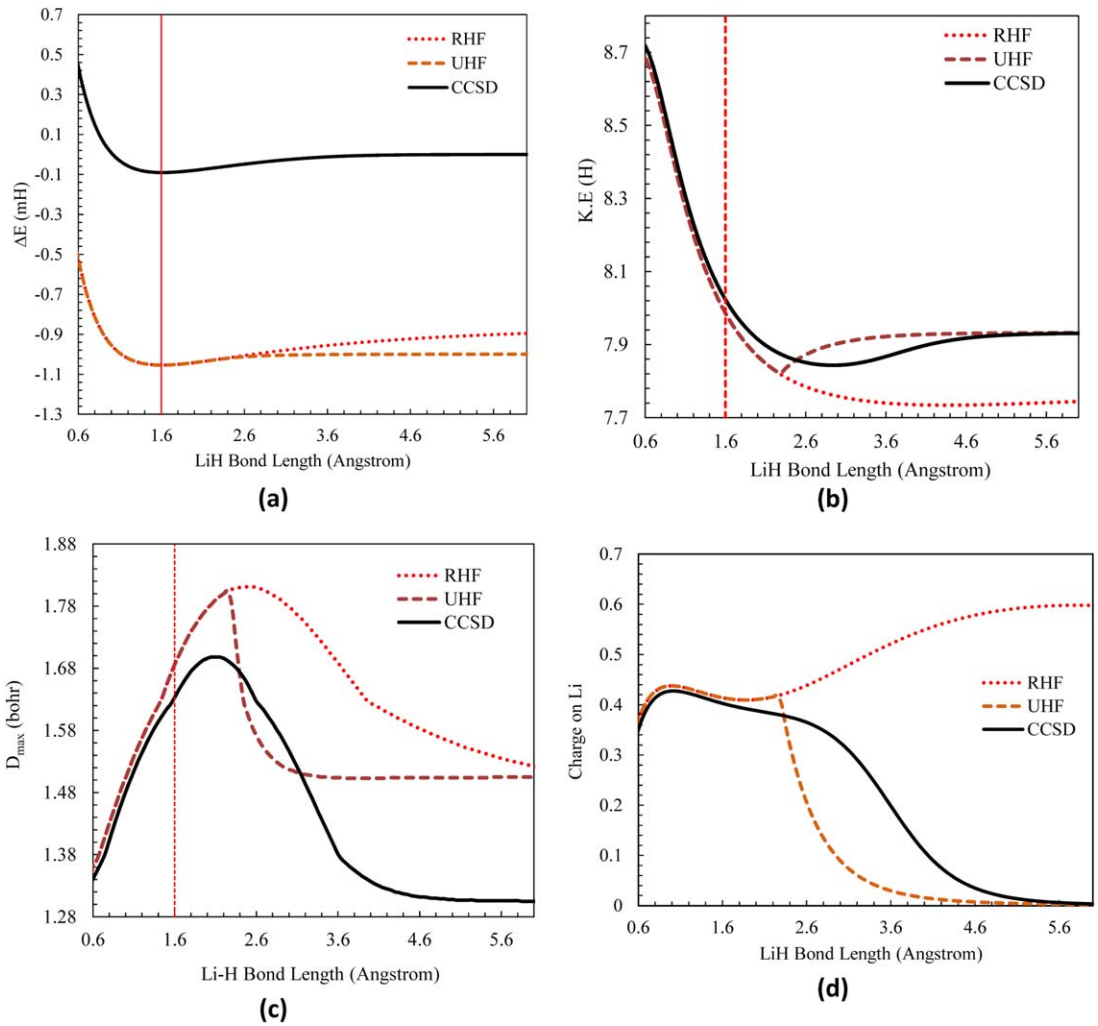

FIGURE 15 ΔE_{bond} (a), KE (b), D_{max} (c), and Hirshfeld charge on Li atom (d) of ground-state $X^1\sum^+$ LiH molecule, plotted versus Li—H bond length. Vertical line denotes the equilibrium bond length

in line with noncovalent interactions between atoms.[98] We thus expect that the EDR will not capture bonding interactions in He_2, and will only highlight Pauli repulsion.

Figure 6 shows the helium dimer's ΔE_{bond}, KE, and D_{max} as functions of bond length. As in Figure 1, trends in D_{max} mirror trends in KE. The KE converges from above to the isolated-atom limit. D_{max} instead shows a tiny peak at modest bond lengths. This artifact of the EDR in nonbonded regions is described in reference 64. Figure 7 shows the He dimer's CCSD bond delocalization shift. As in Figure 2, compressing the bond localizes the electrons, giving a positive peak at small d. Stretching the bond makes the 1-RDM smoothly converge to the isolated-atom limit, such that the bond delocalization shift goes to zero. Plotting the EDR in real space (not shown) gives nearly spherically symmetric regions about each atom. We conclude that, as expected, the 1-RDM and EDR give limited information about the van der Waals interaction.

3.3 | Polar covalent bond: FH

Polar covalent bonds like hydrogen fluoride (FH) have an unequal sharing of electrons[99] but dissociate in the gas phase to neutral atoms.[100] Figure 8 shows the FH molecule's ΔE_{bond}, KE, and D_{max} as functions of bond length. As in Figure 1, trends in D_{max} mirror trends in KE. The KE is similar to H_2: larger than the isolated-atom limit at equilibrium, minimized past equilibrium, and converging in UHF calculations to the isolated-atom limit. D_{max} variations are small, as the system average is dominated by fluorine's localized core electrons. This further highlights the importance of real-space pictures like that in Figure 5.

Figure 9 shows the FH molecule's bond delocalization shift $\Delta\overline{EDR}(FH;d)$. As for H_2, the bond delocalization shift at the equilibrium bond length has a positive peak at small d and a negative peak at large d, highlighting electrons localized in the stable bond.

As for H_2, bond stretching gives fractional occupancy in RHF and CCSD wavefunctions, yielding negative $\Delta\overline{EDR}(FH;d)$ at large bond length and $d = 4$ bohr. One notable difference between FH and H_2 is that the Coulson–Fischer point in FH occurs at relatively short bond lengths. Accordingly, the UHF bond delocalization shift does not show the negative region seen in H_2, but smoothly converges to the isolated-atom limit.

The real-space EDR of stretched FH provides another perspective on this system. Figure 10 shows that at the equilibrium bond length, the relatively localized electrons at $d = 2$ bohr are located between F

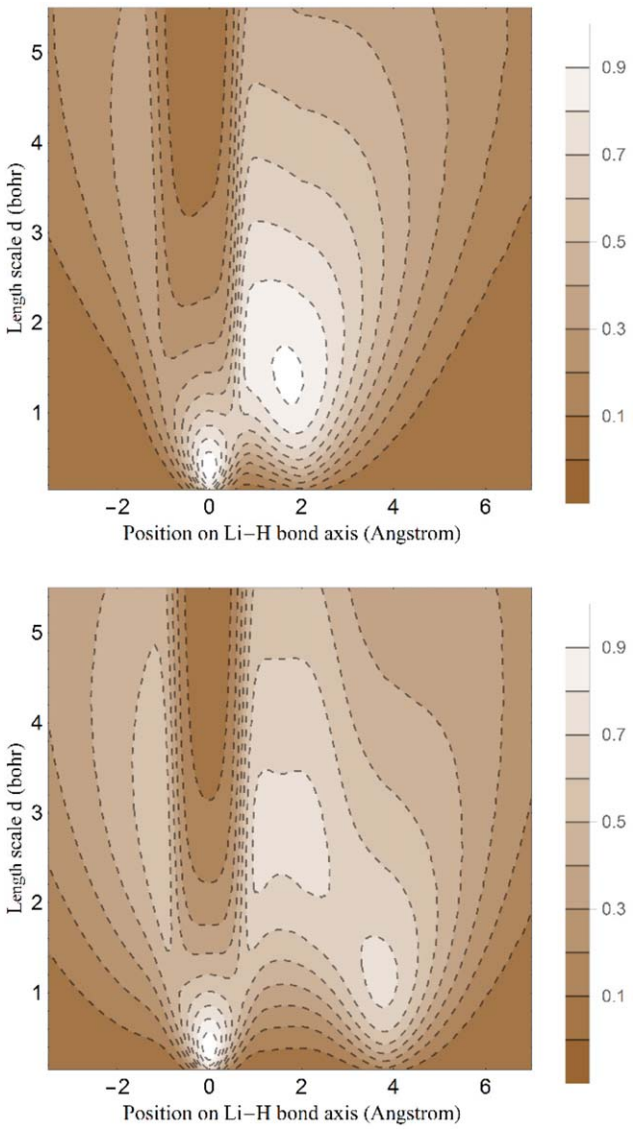

FIGURE 16 CCSD EDR(x, d) of spin-up electrons in stretched LiH at $R = 2.0$Å (top) and at $R = 3.8$ Å (bottom)

and H atoms. Stretching the bond to R= 2.5 Å leaves these relatively localized electrons on F atom. Instead, the relatively delocalized electrons at $d = 4$ bohr are found in the bonding region, and on the H atom. This is consistent with the atomic electronegativities: electrons on H will tend to be bound less tightly than electrons on F.

3.4 | Charge-shift bond: F_2

The F_2 molecule exhibits charge-shift bonding,[3,101] arising largely from resonance between F^+ F^- and F^-F^+ Lewis structures. Like the dipole-dipole fluctuations binding He_2, these charge-charge fluctuations are obvious in the pair density, but less obvious in the 1-RDM. Indeed, a classic symptom of charge-shift bonding is a negligibly small value of the ELF near the bond midpoint.[3] Given this, it is interesting to compare our tools' predictions for charge-shift bonds.

Figure 11 shows the F_2 molecule's ΔE_{bond}, KE, and D_{max} as functions of bond length. Figure 12 shows the corresponding bond

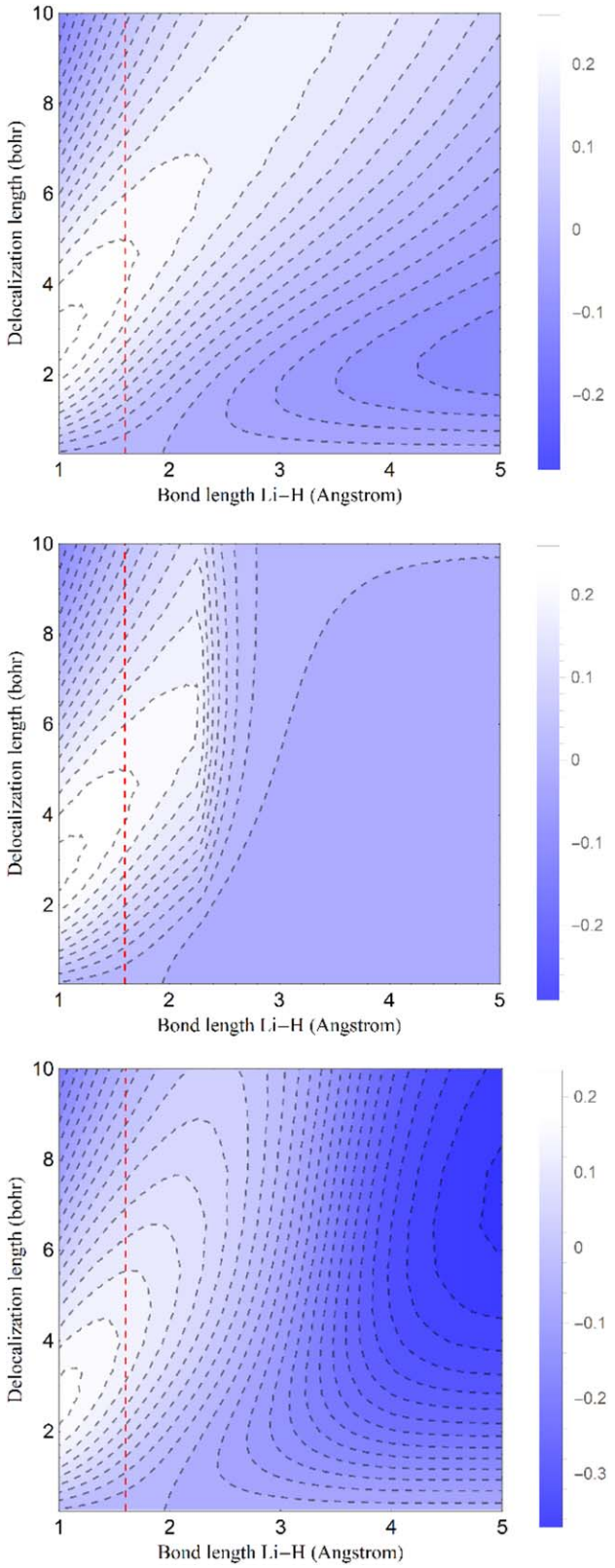

FIGURE 17 Bond delocalization shift $\Delta\overline{\mathrm{EDR}}(\mathrm{LiH}; d)$ of LiH plotted as a function of delocalization distance d and LiH bond length. RHF (top), UHF (middle), CCSD (bottom). Dotted line denotes the equilibrium bond length

delocalization shift. Many of the trends mirror those of H_2, and our discussion here focuses on the most interesting differences. The UHF dissociation curve is unbound, and the Coulson–Fischer point occurs very near the equilibrium bond length. As in FH, this is clearly visible in the UHF bond delocalization shift, which smoothly converges to the isolated-atom limit. The UHF D_{max} converges smoothly to the isolated-atom limit past the Coulson–Fischer point, while the UHF KE exhibits a small local maximum. The RHF and CCSD bond delocalization shifts again highlight the "fractional spin" of the dissociating atoms with a negative peak at small d and large bond length.

Figure 13 shows the EDR in F_2 near equilibrium. Like the ELF, the EDR at small d is quite small in the bonding region, with an "hourglass" shape that appears characteristic of charge-shift bonding.

Stretching the bond past the Coulson–Fischer point (Figure 14) exaggerates this, with the EDR at $d = 1$ Bohr almost completely converged to that of isolated fractional-spin F atoms. The EDR at longer length scales is overall significantly smaller (note the choice of isosurface), highlighting the presence of a small amount of delocalized electron density around the atoms. Finally, the ↑-spin UHF EDR in Figure 14 shows a small degree of symmetry-breaking, highlighting the symmetry-broken solution.

3.5 | Ionic molecule: LiH

LiH has long been a test case for quantum chemistry.[38,102–105] The adiabatic ground state $X^1\sum^+$ of LiH is mostly ionic at the equilibrium bond length, and has increasing covalent character as the bond is stretched.[102] This bonding has been studied by various descriptors[38,102] and is associated with a "harpoon" mechanism.[106]

Figure 15 shows the LiH ΔE_{bond}, KE, and D_{max} as well as the Hirshfeld charge on Li atom as functions of bond length. As in Figure 1, trends in D_{max} mirror trends in KE. Accurate CCSD calculations show that the Hirshfeld charge drops to zero between 2.5 and 4 Angstrom, qualitatively consistent with the QTAIM charges in Figure 2 of reference 102. The RHF singlet instead gives excessive charge transfer in stretched bonds. The CCSD kinetic energy goes through a minimum in this region, and D_{max} goes through a maximum, qualitatively consistent with the corresponding maximum in the shared-electron distribution index.[38,102] The UHF solution shows the by-now familiar discontinuities in KE and D_{max}.

Figure 16 provides a different perspective on this system, showing how the EDR can highlight the back-transfer of electrons from H to Li as the bond is stretched. (Similar plots for H_2 and FH are included as Supporting Information.) For modestly stretched bonds ($R = 2$ Angstrom), the EDR shows a peak in the Li core region at small d, highlighting the localized Li core electrons, and a second peak near the H at most larger d, highlighting the delocalized valence electrons transferred to hydrogen. For further bond stretching ($R = 3.8$ Angstrom), this peak bifurcates into a more localized peak on H, and a more delocalized peak on Li, highlighting the transfer of electrons into the Li atom valence region. This bifurcation is similar to that seen in the ELF in Figure 5 of reference 102, with the added information that the peak near Li is less localized and more diffuse than the peak near H. An animation provided as Supporting Information illustrates how the EDR becomes more delocalized, and more shifted to the Li atom, as the bond is stretched. Figure 17 shows the bond delocalization shift for LiH. As for the other molecules studied, the bond delocalization shift has a positive peak at small delocalization lengths and a negative peak at large delocalization lengths, highlighting how bond formation makes the electrons more localized and more tightly bound.

The RHF and CCSD bond delocalization shifts show fractional occupancy effects at large bond lengths. The UHF bond delocalization shifts clearly indicates the abrupt changes at the Coulson–Fischer point, and shows the expected smooth convergence to the isolated-atom limit on further bond stretching.

4 | CONCLUSIONS

The results presented in this work illustrate how the electron delocalization range can give insight into bond dissociation. The system-averaged delocalization length D_{max} largely mirrors trends in the system-averaged kinetic energy. Bond delocalization shifts quantifies effects of delocalization and fractional occupancy in stretched bonds, providing a more detailed picture. Isosurfaces of the EDR itself, plotted at delocalization lengths identified in the bond delocalization shift, highlight chemically interesting regions of space. We conclude that the EDR provides a novel perspective on bond dissociation.

ACKNOWLEDGMENT

This work was supported in part by funds from Texas Christian University.

REFERENCES

[1] A. I. Boldyrev, L. S. Wang, *Chem. Rev.* **2005**, *105*, 3716.

[2] P. Politzer, J. S. Murray, T. Clark, *Phys. Chem. Chem. Phys.* **2013**, *15*, 11178.

[3] S. Shaik, D. Danovich, B. Silvi, D. L. Lauvergnat, P. C. Hiberty, *Chemistry* **2005**, *11*, 6358.

[4] A. J. Cohen, P. Mori-Sánchez, W. Yang, *Chem. Rev.* **2012**, *112*, 289.

[5] J. W. Hollett, L. K. McKemmish, P. M. W. Gill, *J. Chem. Phys.* **2011**, *134*, 224103.

[6] V. A. Rassolov, M. A. Ratner, J. A. Pople, *J. Chem. Phys.* **2000**, *112*, 4014.

[7] J. VandeVondele, M. Sprik, *Phys. Chem. Chem. Phys.* **2005**, *7*, 1363.

[8] M. Hellgren, F. Caruso, D. R. Rohr, X. Ren, A. Rubio, M. Scheffler, P. Rinke, *Phys. Rev. B* **2015**, *91*, 165110.

[9] G. E. Scuseria, H. F. Schaefer, *Chem. Phys. Lett.* **1990**, *174*, 501.

[10] A. D. Becke, M. R. Roussel, *Phys. Rev. A* **1989**, *39*, 3761.

[11] J. Gerratt, D. L. Cooper, P. B. Karadakov, M. Raimondi, *Chem. Soc. Rev.* **1997**, *26*, 87.

[12] Y. Mo, L. Song, W. Wu, Z. Cao, Q. Zhang, *J. Theor. Comput. Chem.* **2002**, *01*, 137.

[13] Y. Mo, S. D. Peyerimhoff, *J. Chem. Phys.* **1998**, *109*, 1687.

[14] J. P. Foster, F. Weinhold, *J. Am. Chem. Soc.* **1980**, *102*, 7211.

[15] R. L. Fulton, *J. Phys. Chem. A* **2004**, *108*, 11691.

[16] D. Y. Zubarev, A. I. Boldyrev, *Phys. Chem. Chem. Phys.* **2008**, *10*, 5207.

[17] R. F. W. Bader, *Chem. Rev.* **1991**, *91*, 893.

[18] R. F. W. Bader, *Atoms in Molecules: A Quantum Theory*, Clarendon Press: Oxford, **1994**.

[19] K. Wagner, M. Kohout, *Theor. Chem. Acc.* **2010**, *128*, 39.

[20] W. Scherer, P. Sirsch, D. Shorokhov, M. Tafipolsky, G. S. McGrady, E. Gullo, *Chemistry* **2003**, *9*, 6057.

[21] P. de Silva, J. Korchowiec, T. A. Wesolowski, *ChemPhysChem* **2012**, *13*, 3462.

[22] H. Schmider, K. E. Edgecombe, V. H. Smith, W. Weyrich, *J. Chem. Phys.* **1992**, *96*, 8411.

[23] J. Sandoval-Lira, M. Hô, R. Hernández-Esparza, J. C. Ramírez, J. M. Hernández-Pérez, *Theor. Chem. Acc.* **2016**, *135*, 1.

[24] S. R. Gadre, S. A. Kulkarni, R. K. Pathak, *Phys. Rev. A* **1989**, *40*, 4224.

[25] P. W. Anderson, *Phys. Rev.* **1969**, *181*, 25.

[26] V. V. Karasiev, R. S. Jones, S. B. Trickey, F. E. Harris, *Phys. Rev. B* **2009**, *80*, 245120.

[27] R. F. W. Bader, A. Streitwieser, A. Neuhaus, K. E. Laidig, P. Speers, *J. Am. Chem. Soc.* **1996**, *118*, 4959.

[28] R. F. W. Bader, M. E. Stephens, *J. Am. Chem. Soc.* **1975**, *97*, 7391.

[29] W. Weyrich, *Acta Crystallogr. Sect. A* **1987**, *43*, C320.

[30] E. Hückel, *Z. Phys.* **1931**, *70*, 204.

[31] I. Mayer, *Chem. Phys. Lett.* **1983**, *97*, 270.

[32] K. B. Wiberg, *Tetrahedron* **1968**, *24*, 1083.

[33] S. Tretiak, S. Mukamel, *Chem. Rev.* **2002**, *102*, 3171.

[34] M. Head-Gordon, A. M. Grana, D. Maurice, C. A. White, *J. Phys. Chem.* **1995**, *99*, 14261.

[35] F. Plasser, M. Wormit, A. Dreuw, *J. Chem. Phys.* **2014**, *141*, 024106.

[36] J. Cioslowski, S. T. Mixon, *J. Am. Chem. Soc.* **1991**, *113*, 4142.

[37] R. L. Fulton, S. T. Mixon, *J. Phys. Chem.* **1993**, *97*, 7530.

[38] R. Ponec, D. L. Cooper, *J. Mol. Struct.: Theochem* **2005**, *727*, 133.

[39] R. F. W. Bader, G. L. Heard, *J. Chem. Phys.* **1999**, *111*, 8789.

[40] L. L. R. C. Bocchicio, A. Torre, *Chem. Phys. Lett.* **2003**, *374*, 567.

[41] R. L. Fulton, S. T. Mixon, *J. Phys. Chem.* **1995**, *99*, 9768.

[42] P. Bultinck, D. L. Cooper, R. Ponec, *J. Phys. Chem. A* **2010**, *114*, 8754.

[43] D. R. Alcoba, L. Lain, A. Torre, R. C. Bochicchio, *J. Chem. Phys.* **2005**, *123*, 144113.

[44] D. Vanfleteren, D. Van Neck, P. Bultinck, P. W. Ayers, M. Waroquier, *J. Chem. Phys.* **2012**, *136*, 014107.

[45] D. Vanfleteren, D. Van Neck, P. Bultinck, P. W. Ayers, M. Waroquier, *J. Chem. Phys.* **2010**, *132*, 164111.

[46] A. Savin, R. Nesper, S. Wengert, T. F. Fässler, *Angew. Chem. Int. Ed. Engl.* **1997**, *36*, 1808.

[47] A. D. Becke, K. E. Edgecombe, *J. Chem. Phys.* **1990**, *92*, 5397.

[48] A. Savin, A. D. Becke, J. Flad, R. Nesper, H. Preuss, H. G. von Schnering, *Angew. Chem. Int. Ed. Engl.* **1991**, *30*, 409.

[49] F. Feixas, E. Matito, M. Duran, M. Sola, B. Silvi, *J. Chem. Theory Comput.* **2010**, *6*, 2736.

[50] X. Fradera, M. A. Austen, R. F. W. Bader, *J. Phys. Chem. A* **1999**, *103*, 304.

[51] E. R. Johnson, S. Keinan, P. Mori-Sánchez, J. Contreras-García, A. J. Cohen, W. Yang, *J. Am. Chem. Soc.* **2010**, *132*, 6498.

[52] R. F. W. Bader, C. Gatti, *Chem. Phys. Lett.* **1998**, *287*, 233.

[53] D. W. Szczepanik, E. Żak, K. Dyduch, J. Mrozek, *Chem. Phys. Lett.* **2014**, *593*, 154.

[54] M. Kohout, *Int. J. Quantum Chem.* **2004**, *97*, 651.

[55] E. Matito, M. Sola, P. Salvador, M. Duran, *Faraday Discuss.* **2007**, *135*, 325.

[56] H. Schmider, *J. Chem. Phys.* **1996**, *105*, 11134.

[57] H. L. Schmider, A. D. Becke, *J. Mol. Struct.: Theochem* **2000**, *527*, 51.

[58] H. L. Schmider, A. D. Becke, *J. Chem. Phys.* **2002**, *116*, 3184.

[59] A. D. Becke, *J. Chem. Phys.* **2003**, *119*, 2972.

[60] E. P. A. F. L. A. J. Kong, *Phys. Rev. A* **2013**, *88*,

[61] E. I. Proynov, *J. Mol. Struct.: Theochem* **2006**, *762*, 159.

[62] K. Takatsuka, T. Fueno, K. Yamaguchi, *Theor. Chim. Acta (Berl.)* **1978**, *48*, 175.

[63] B. G. Janesko, G. Scalmani, M. J. Frisch, *J. Chem. Phys.* **2014**, *141*, 144104.

[64] B. G. Janesko, G. Scalmani, M. J. Frisch, *Phys. Chem. Chem. Phys.* **2015**, *17*, 18305.

[65] B. G. Janesko, G. Scalmani, M. J. Frisch, *J. Chem. Theory Comput.* **2016**, *12*, 79.

[66] B. G. Janesko, K. B. Wiberg, G. Scalmani, M. J. Frisch, *J. Chem. Theory Comput.* **2016**, *12*, 3185.

[67] B. G. Janesko, *J. Comput. Chem.* **2016**, *37*, 1993.

[68] P. Mori-Sánchez, A. J. Cohen, *J. Chem. Phys.* **2014**, *141*, 164124.

[69] W. Yang, P. Mori-Sánchez, A. J. Cohen, *J. Chem. Phys.* **2013**, *139*, 104114.

[70] P. Hohenberg, W. Kohn, *Phys. Rev.* **1964**, *136*, B864.

[71] W. Kohn, L. J. Sham, *Phys. Rev.* **1965**, *140*, A1133.

[72] A. D. Becke, *Phys. Rev. A* **1988**, *38*, 3098.

[73] J. P. Perdew, Y. Wang, *Phys. Rev. B* **1992**, *45*, 13244.

[74] A. D. Becke, *J. Chem. Phys.* **1992**, *97*, 9173.

[75] P. J. Stephens, F. J. Devlin, C. F. Chabalowski, M. J. Frisch, *J. Phys. Chem.* **1994**, *98*, 11623.

[76] R. Seeger, J. A. Pople, *J. Chem. Phys.* **1977**, *66*, 3045.

[77] N. C. Handy, H. F. Schaefer, *J. Chem. Phys.* **1984**, *81*, 5031.

[78] K. B. Wiberg, C. M. Hadad, T. J. LePage, C. M. Breneman, M. J. Frisch, *J. Phys. Chem.* **1992**, *96*, 671.

[79] T. H. Dunning, *J. Chem. Phys.* **1989**, *90*, 1007.

[80] D. E. Woon, T. H. Dunning, *J. Chem. Phys.* **1994**, *100*, 2975.

[81] M. J. Frisch, G. W. Trucks, H. B. Schlegel, G. E. Scuseria, M. A. Robb, J. R. Cheeseman, G. Scalmani, V. Barone, B. Mennucci, G. A. Petersson, H. Nakatsuji, M. Caricato, X. Li, H. P. Hratchian, J. Bloino, B. G. Janesko, A. F. Izmaylov, A. Marenich, F. Lipparini, G. Zheng, J. L. Sonnenberg, W. Liang, M. Hada, M. Ehara, K. Toyota, R. Fukuda, J. Hasegawa, M. Ishida, T. Nakajima, Y. Honda, O. Kitao, H. Nakai, T. Vreven, K. Throssell, J. A. Montgomery, Jr.J. E. Peralta, F. Ogliaro, M. Bearpark, J. J. Heyd, E. Brothers, K. N. Kudin, V. N. Staroverov, T. Keith, R. Kobayashi, J. Normand, K. Raghavachari, A. Rendell, J. C. Burant, S. S. Iyengar, J. Tomasi, M. Cossi, N. Rega, J. M. Millam, M. Klene, J. E. Knox, J. B. Cross, V. Bakken, C. Adamo, J. Jaramillo, R. Gomperts, R. E. Stratmann, O. Yazyev, A. J. Austin, R. Cammi, C. Pomelli, J. W. Ochterski, R. L. Martin, K. Morokuma, V. G. Zakrzewski, G. A. Voth, P. Salvador, J. J. Dannenberg, S. Dapprich, P. V. Parandekar, N. J. Mayhall, A. D. Daniels, O. Farkas, J. B. Foresman, J. V. Ortiz, J. Cioslowski, D. J. Fox, Gaussian Development Version, Revision I.02+; Gaussian, Inc., Wallingford, CT, USA, **2014**.

[82] G. B. Bacskay, *Chem. Phys.* **1981**, *61*, 385.

[83] D. K. W. Mok, R. Neumann, N. C. Handy, *J. Phys. Chem.* **1996**, *100*, 6225.

[84] J. K. Burdett, T. A. McCormick, *J. Phys. Chem. A* **1998**, *102*, 6366.

[85] H. C. Bowen, J. W. Linnett, *J. Chem. Soc. (Resumed)* **1963**, 1064.

[86] C. A. Coulson, R. P. Bell, *Trans. Faraday Soc.* **1945**, *41*, 141.

[87] M. W. Schmidt, J. Ivanic, K. Ruedenberg, in *The Chemical Bond*, Wiley-VCH Verlag GmbH & Co. KGaA, **2014**, pp. 1–68.

[88] J. R. Walton, L. A. Rivera−Rivera, R. R. Lucchese, J. W. Bevan, *J. Phys. Chem. A* **2016**, *120*, 817.

[89] G. B. Bacskay, S. Nordholm, *J. Phys. Chem. A* **2013**, *117*, 7946.

[90] K. Ruedenberg, M. W. Schmidt, *J. Comput. Chem.* **2007**, *28*, 391.

[91] C. W. Wilson, W. A. Goddard, *Theor. Chim. Acta* **1972**, *26*, 195.

[92] K. Ruedenberg, *Rev. Mod. Phys.* **1962**, *34*, 326.

[93] S. Nordholm, *J. Chem. Educ.* **1988**, *65*, 581.

[94] G. B. Bacsckay, S. Nordholm, *J. Phys. Chem. A* **2013**, *117*, 7946.

[95] K. Ruedenberg, *Rev. Mod. Phys.* **1962**, *34*, 326.

[96] A. J. Cohen, P. Mori-Sánchez, W. Yang, *Science* **2008**, *321*, 792.

[97] F. Luo, G. C. McBane, G. Kim, C. F. Giese, W. R. Gentry, *J. Chem. Phys.* **1993**, *98*, 3564.

[98] M. García-Revilla, P. L. A. Popelier, E. Francisco, Á. Martín Pendás, *J. Chem. Theory Comput.* **2011**, *7*, 1704.

[99] R. T. Sanderson, *Science* **1951**, *114*, 670.

[100] J. P. Perdew, R. G. Parr, M. Levy, J. L. Balduz, *Phys. Rev. Lett.* **1982**, *49*, 1691.

[101] S. Shaik, P. Maitre, G. Sini, P. C. Hiberty, *J. Am. Chem. Soc.* **1992**, *114*, 7861.

[102] M. Rodríguez-Mayorga, E. Ramos-Cordoba, P. Salvador, M. Solà, E. Matito, *Mol. Phys.* **2016**, *114*, 1345.

[103] B. Weiner, Y. Ohrn, *J. Phys. Chem.* **1987**, *91*, 563.

[104] R. S. Mulliken, *Phys. Rev.* **1936**, *50*, 1017.

[105] R. Ponec, D. L. Cooper, *Faraday Discuss.* **2007**, *135*, 31.

[106] J. C. Polanyi, A. H. Zewail, *Acc. Chem. Res.* **1995**, *28*, 119.

SUPPORTING INFORMATION

Additional Supporting Information can be found in the online version of this article at the publisher's website.

How to cite this article: A. Mehmood, B. G. Janesko. *Int. J. Quantum Chem.* **2016**, *116*, 1783–1795. DOI: 10.1002/qua.25225